Microstructure Investigation of Thermally Induced Phase Transformation in Fe–Mn–Mo–Si Alloys

Osman ARMAĞAN*[1] , Talip KIRINDI[2]

[1]Karamanoğlu Mehmetbey Üniversitesi, Sağlık Hizmetleri Meslek Yüksekokulu, Tıbbi Hizmetler ve Teknikler Bölümü, Optisyenlik Programı, 70200, Karaman, Türkiye
[2]Kırıkkale Üniversitesi, Eğitim Fakültesi, Eğitim Bilimleri ve Matematik Bölümü, 71450, Kırıkkale, Türkiye

Abstract: In this study, structural and crystallographic properties of phase transformations in Fe–Mn– Mo-Si (Mn = 15.14 wt.% and 18.45 wt.%) alloys were investigated. The effects of heat treatment temperature on microstructure were investigated by Scanning Electron Microscopy (SEM) and Metallurgical Microscopy (MM). In addition to this, crystallographic properties of phase transformations were revealed by using Transmission Electron Microscopy (TEM) and X–Ray Diffraction (XRD) methods. In the samples subjected to heat treatment at 750 °C, it was observed that bainite structure was formed in the alloy where Mn amount was low and ferrite structure in the alloy where Mn amount was higher. In addition, it was found that both alloys heat–treated at 900 °C had the same microstructure (pearlite structure) in SEM and MM microscopy. At the same time, microstructure observations revealed that bainite and pearlite structures contain a mixture of ferrite and cementite. In the TEM studies it was revealed by electron diffraction pattern analyses that bainite and ferrite phase crystallized in b.c.c. structure and cementite phase in orthorhombic structure. $\gamma \rightarrow \alpha$ type transformation was observed for α–bainite formation, and orientation relationship was found as $(\bar{1}11)_\gamma // (011)_\alpha$, $[101]_\gamma // [\bar{1}1\bar{1}]_\alpha$.

Fe-Mn-Mo-Si Alaşımlarında Termal Etkili Faz Dönüşümlerinin Mikro Yapı İncelemeleri

Anahtar Kelimeler
Beynit,
Ferrit,
Sementit,
Perlit,
Kristalografik özellikler,
TEM

Özet: Bu çalışmada, Fe-%XMn-Mo-Si (X=15,14 ve 18,45) alaşımlarında termal etki ile meydana gelen faz dönüşümlerinin yapısal ve kristalografik özellikleri incelenmiştir. Isıl işlem sıcaklığının mikro yapısı üzerine etkileri Taramalı Elektron Mikroskobu (SEM) ve Metalürji Mikroskobu (MM) incelemeleri ile yapıldı. Bunun yanı sıra kristalografik özellikleri ise Geçirmeli Elektron Mikroskobu (TEM) ve X-Işınları Kırınımı (XRD) yöntemleri kullanılarak ortaya çıkarılmıştır. 750 °C' de ısıl işleme tabi tutulan numunelerde Mn miktarının az olduğu alaşımda beynit yapı oluşurken Mn miktarının daha fazla olduğu alaşımda ferrit yapının oluştuğu gözlendi. Ek olarak, 900 °C'de ısıl işlem görmüş her iki alaşımın da SEM ve MM mikroskopisinde aynı mikro yapıya (perlit yapı) sahip olduğu bulundu. Aynı zamanda, beynit ve perlit yapılarının ferrit ve sementit karışımını içerdiği mikro yapı gözlemleri ile ortaya konuldu. TEM incelemelerinde elektron kırınım deseni analizleri sayesinde beynit ve ferrit fazın b.c.c. yapısında, sementit fazın ise ortorombik yapıda kristalleştiği ortaya konuldu. α-beynit oluşumu için $\gamma \rightarrow \alpha$ türü dönüşüm gözlendi ve dönme bağımlılığı $(\bar{1}11)_\gamma // (011)_\alpha$, $[101]_\gamma // [\bar{1}1\bar{1}]_\alpha$ olarak bulundu.

1. Introduction

Nowadays, the most important reason for the use of Fe based alloys in numerous industrial applications is their mechanical properties. The development of

these properties due to the changes in the microstructure of the alloys has been the subject of many studies [1, 2]. The reason for the changes in mechanical and physical properties caused by the applied deformation or thermal effect can only be

explained by considering the internal structure. On the other hand, various physical methods such as heat treatment applications, deformation applications, cold forming and quenching have been applied in industry, especially in metal alloys, in order to adjust according to requirements by changing internal structure [3–8]. The microstructures of the same type of Fe based alloys formed by casting, heat treatment or deformation are formed in very different structures according to the applied process conditions, and these different structures are reflected in the physical properties in different ways [1]. Besides, the composition of the alloys is highly effective on the type and formation of phase transformations that occur with the effect of thermal and deformation. Particularly in Fe–Mn based alloys, diffusion and non–diffusion phase transformations occur due to physical effects or alloy composition. In iron and steel alloys, phases such as bainite, ferrite, cementite occur during diffusion and non–diffusion phase transformations. At the same time, martensite structures in such alloys are formed only by non–diffusion phase transformations [6–8].

Microstructures in steel, iron and cast iron have a ferrite, pearlite, bainite, cementite, martensite and austenite phase, however, only a few commercial steels have a fully ferrite phase [5, 9–14]. In experimental applications, it is observed that austenite structure is transformed into bainite as a result of transformation of Fe based alloys by an isothermal cooling [5, 11]. Furthermore, the bainite structure is a diffusion or non–diffusive phase transformation under high conversion temperatures [15]. The bainite structure, which is defined as supersaturated ferrite, exhibits a cubic structure like ferrite in crystallographic form. In many studies, crystallographic orientation relations of austenite–bainitic ferrite phase transformations in steel type alloys have been found as G–T (Greninger–Troiano), N–W (Nishiyama–Wassermann), K–S (Kurdjumov–Sachs) [16–18]. In addition, in the formation of bainite, carbide–containing alloying elements such as Mo, Cr and V, which are added to low–carbon alloys, are known to transform the structure into bainitic [19].

Klier and Lymen stated that this meant that austenite became compound unstable before it became a bainite, divided into carbon–rich and carbon–depleted volumes [20]. According to Bhadesiha, the carbon–low regions must be transformed into the over–saturated bainite with a subsequent martensite–like knitting arrangement shortly after the iron carbide precipitation [21]. M. X. Zhang and P. M. Kelly examined the structural and crystallographic properties of martensite and bainite structures formed as product phase in their study on Fe–20 wt.%Ni–6wt.%Mn–0.009wt.%C and Fe–19wt.%Ni–3.5wt.%Mn–0.009wt.%C alloys. By applying isothermal conversion method, they observed the alloy containing 6 wt.% Mn ratio in the martensite structure (-70 °C) while observing the formation of bainite structure (400 °C) in the alloy containing 3.5 wt.% Mn ratio [22]. L. C. Chang has done a study on the Fe–2.12wt.%Mn–2wt.%Ni–1.77wt.%Si–0.1wt.% C, Fe–2.16wt.%Mn–2.07wt.%Ni–2.01wt.%Si–0.27 wt.%C and Fe–2.15wt.%Mn–2.10wt.%Si–0.46wt.%C alloys, and he investigated the microstructure and transformation reaction kinetics of upper and lower bainite in high–medium to low–grade C and also in high Si ratios [15]. In some studies, it is reported that bainite has a diffusion and non–diffusion phase transformation occurring at high conversion temperatures and also reported the formation of cementite in the lower bainite [12, 23]. Lee and et al., the acicular ferrite and allotriomorphic structures have been observed in Fe–2.05wt.%Si–3.07wt.%Mn–0.7wt.%Mo–0.22wt.%C alloy when different heat treatment temperatures and different heat treatment times were applied. In addition, they have been explained the crystallography of this product phases [24]. The effect of Co (wt%) on the microstructure and mechanical properties of low Cr-W Steels with a very low Mn(wt %) and C (wt %) ratio was studied, and microstructure analysis revealed martensite, bainite, and precipitates clearly [25]. As with chrome molybdenum (tungsten) [Cr-Mo (W)] Steels, bainite and martensite structures are formed depending on the amount of Cr (wt%) in steels with different compositions [26].

Almost all of the previous studies have been done under diffusion phase transformations and usually in percent (by mass) certain carbon ratios (low, medium and high) at steel alloys. In particular, in this study, microstructures formed depending on the amount of Mn are examined in Fe-Mn-Mo-Si alloys with a high Mn(wt) ratio. It is aimed to produce product phases (bainite, ferrite, etc.) which are obtained by diffusion phase transformations in steel alloys, general, in Fe–Mn based alloys i.e. steel alloys with much less percent of carbon ratios (C<0.05) and diffusion less phase transformations.

2. Material and Method

2.1. Experimental

The alloys employed in the present study were prepared in TÜBİTAK-Gebze by vacuum induction melting under an argon atmosphere from pure (99.9%) alloying elements. The chemical composition (wt.%) of the alloys is given in Table 1. These chemical rates were determined using Electron Dispersion Spectroscopy (EDS). The ingot-shaped alloys were cut with a diamond cutter at room temperature. The samples were sealed into evacuated quartz tubes and then heat treated. Samples placed in vacuumed silica tubes were put in an oven at room temperature and increased by 10 degrees per minute to 750 and 900 degrees and

Table 1. Chemical composition of the studied alloys (wt.%)

Alloys (wt.%)	Chemical compositions (wt.%)				
	Fe	Mn	Mo	Si	C
Fe-15.14 Mn-5.10 Mo-2.18 Si (A)	77.17	15.14	5.10	2.18	0.015
Fe-18.45 Mn-4.69 Mo-1.99 Si (B)	74.43	18.45	4.69	1.99	0.048

Table 2. Heat treatments of alloys

Samples	Nature of heat treatments
A_1, B_1	Homogenized at 750 °C for 2 h and quenched in water bath at room temperature
A_2, B_2	Homogenized at 900 °C for 2 h and quenched in water bath at room temperature

annealed at these temperatures for 2 hours. The heat treatments of sealed samples were given in Table 2. Samples taken from the oven were subjected to rapid cooling by breaking the silica tubes and throwing them into water at room temperature without wasting time. For SEM studies, first the surfaces of the samples were mechanically polished and then made ready to be imaged by etching in a solution consisting of 5% nitric acid and 95% methanol for 30 s. For SEM observations, a JEOL 5600 device operated at 20 kV were used. EDS analyzes were performed while micro photographs were taken from samples prepared for SEM examination. For Metallurgical Microscopy (MM) analyzes, samples were subjected to mechanical cleaning, and picric acid solution (4 g of picric acid and 100 ml ethanol) was used for the etching of the surface cleaned and polished samples. Picric acid solution was used to obtain color micro photographs with MM.

For the TEM studies, samples cut from ingot-shaped alloys with a diamond cutter were highly thinned with emery papers. These samples were prepared with a diameter of 3mm and a thickness of 50-60 μm. Then for these samples were prepared a solution consisting of 90% acetic acid and 10% perchloric acid. With this solution, double jet electro–polishing (drilling) were applied in the Streurs-tenupol Jet unit at a temperature of between -15 °C to 10 °C and with a voltage of 20V. In the TEM study, a JEOL 3010 device was used operating at 300 kV.

Volume fractions of α (bainite, ferrite) and θ cementites phases were measured by XRD method. The Rigaku Geigerflex D–MaxB X–Ray diffractometer was used as the XRD device (Cu Kα radiation and monochromatic from an angle of 20–80° (2θ) with a step size of 0.02° 2θ and a counting time of 6 s step^{-1}). In previous studies, lattice parameters were calculated using the following formula:

$$a_\gamma = \frac{\lambda\sqrt{h^2k^2l^2}}{2sin\theta_{hkl}} \qquad (1)$$

where λ, (hkl), and θ_{hkl} are the wavelength of the radiation, the three Miller indices of a plane and the Bragg angle, respectively [27, 28].

3. Results and Discussion

3.1. Investigation of phases morphology

The SEM and MM images of the A_1 sample were given in Figure 1a and b respectively. In micro photographs, bainitic–ferrite lamellae and precipitates formed at the grain boundary were shown regionally. Bainitic–ferrite (BF), one of the varieties of bainite, was formed in the form of lamellae and the heat treatment temperature was found to be effective in this formation [21]. As can be seen from the two pictures, the most important feature of the bainite phase is that carbides are present as separate particles. In the SEM image given in Figure 1a, bainitic–ferrite lamellae appear to form in parallel to each other in some regions. However, it was seen that the lamella sets in these different orientations could not continue their extension in the regions where they intersected. In addition, a micro–mixture consisting of the so–called austenite phase (black regions) and retained austenite (RA) was observed in the regions where the energy required for the bainitic transformation was not achieved [29]. Ferrite has needle morphology, and carbides are individual particles at bainite phase. Due to these morphological differences, bainite has important characteristics. In general, the bainite is rich in carbon, has a high strength and toughness, and has a complex morphology [10]. Si as an alloying element, in bainite, is an element that suppresses a two–phase holding them precipitate cementite microstructure [30]. The transition of Si to iron is higher at high temperatures and the effect of Si is reduced due to the homogenization temperature which is not high enough in this sample [31, 32]. Mo, which is not an easily soluble element in γ and α phase formed in iron based alloys, is a strong carbide–forming element [33–35]. This effect is more clearly seen due to the high Mo ratio in this alloy. Each of the alloying elements can be considered to have effects on the phase conversion temperature of the alloy and on the percentage of carbon required for conversion.

Austenite grain size has a significant effect on the mechanical properties and phase transformations of metals. Barford, Owen and Umemoto et al. reported that bainite reaction rate increased with decreasing
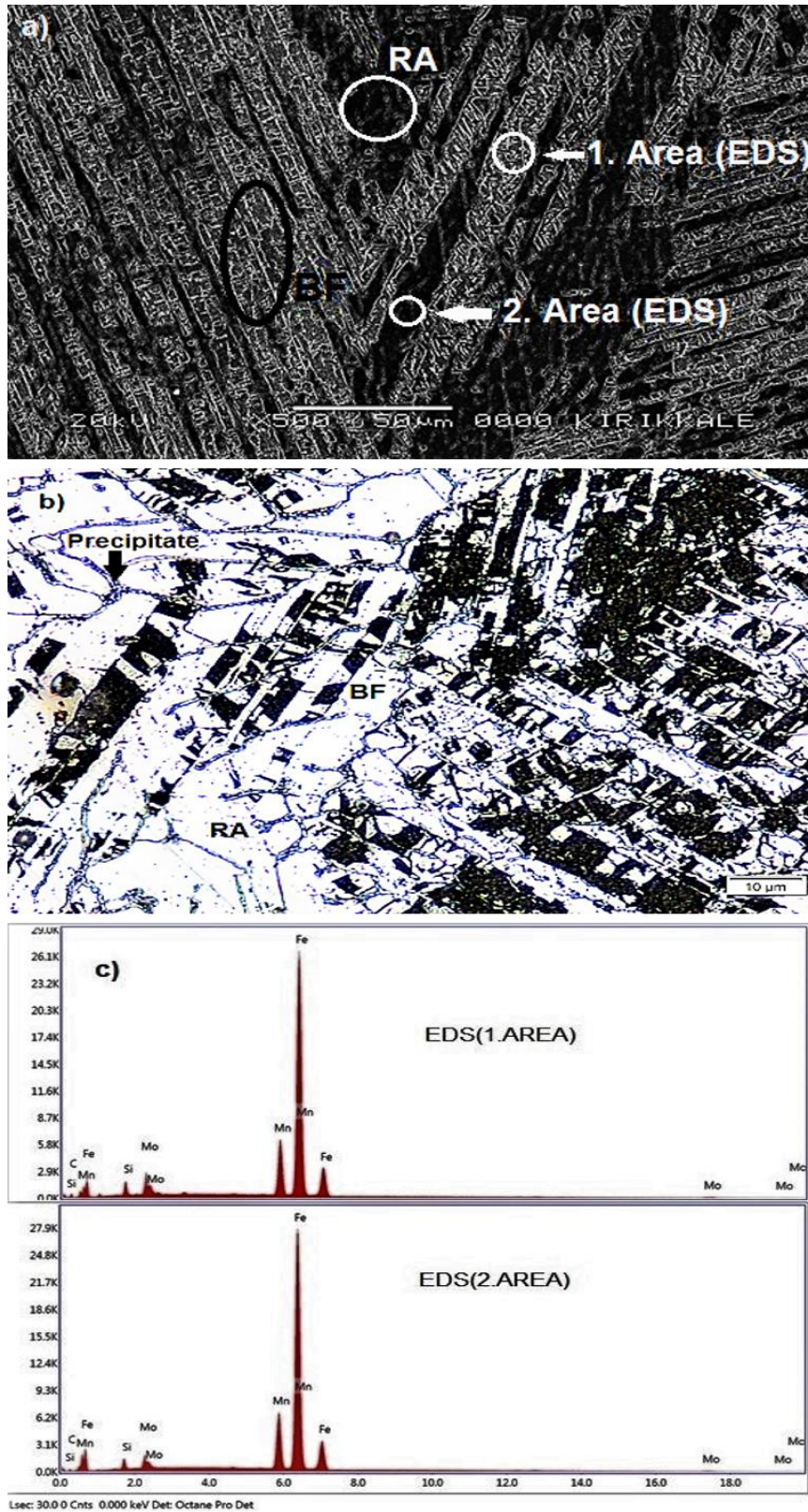
Figure 1. Bainitic-ferrite (BF) lamellae belonging to A_1 sample and microstructure images showing selected areas for EDS (a) SEM, (b) MM (RA : Retained Austenite), (c) EDS peaks taken from selected regions

austenite grain size [36, 37], while Graham and Axon suggested that a good austenite grain structure should delay the development of bainite [38].

By adding elements C, Mn and Cr to the alloy, the starting temperature of the bainite can be reduced. At the same time, the stability of austenite can be increased [30]. Due to the high Mn ratio in the sample, it is not possible to say that bainite formation has occurred in all of the structure, because the remaining regions in the austenite phase are caused by the stabilizing feature of Mn in austenite. Bainite

Table 3. EDS analysis datas

Elements		Fe (wt.%)	Mn (wt.%)	Mo (wt.%)	Si (wt.%)	C (wt.%)	Total (wt.%)
A_1	1. Area	76.60	17.20	3.74	1.93	0.53	100
	2. Area	79.74	18.22	0.23	1.58	0.30	100
B_1	1. Area	61.17	16.13	15.81	5.88	1.01	100
	2. Area	73.77	22.30	2.18	1.63	0.12	100
A_2	1. Area	69.72	16.55	8.41	5.003	0.32	100
	2. Area	76.93	18.48	0.29	3.94	0.36	100
	3. Area	75.29	18.18	3.38	2.91	0.24	100
B_2	1. Area	64.40	17.75	12.01	5.53	0.31	100
	2. Area	72.50	21.20	3.63	2.52	0.15	100
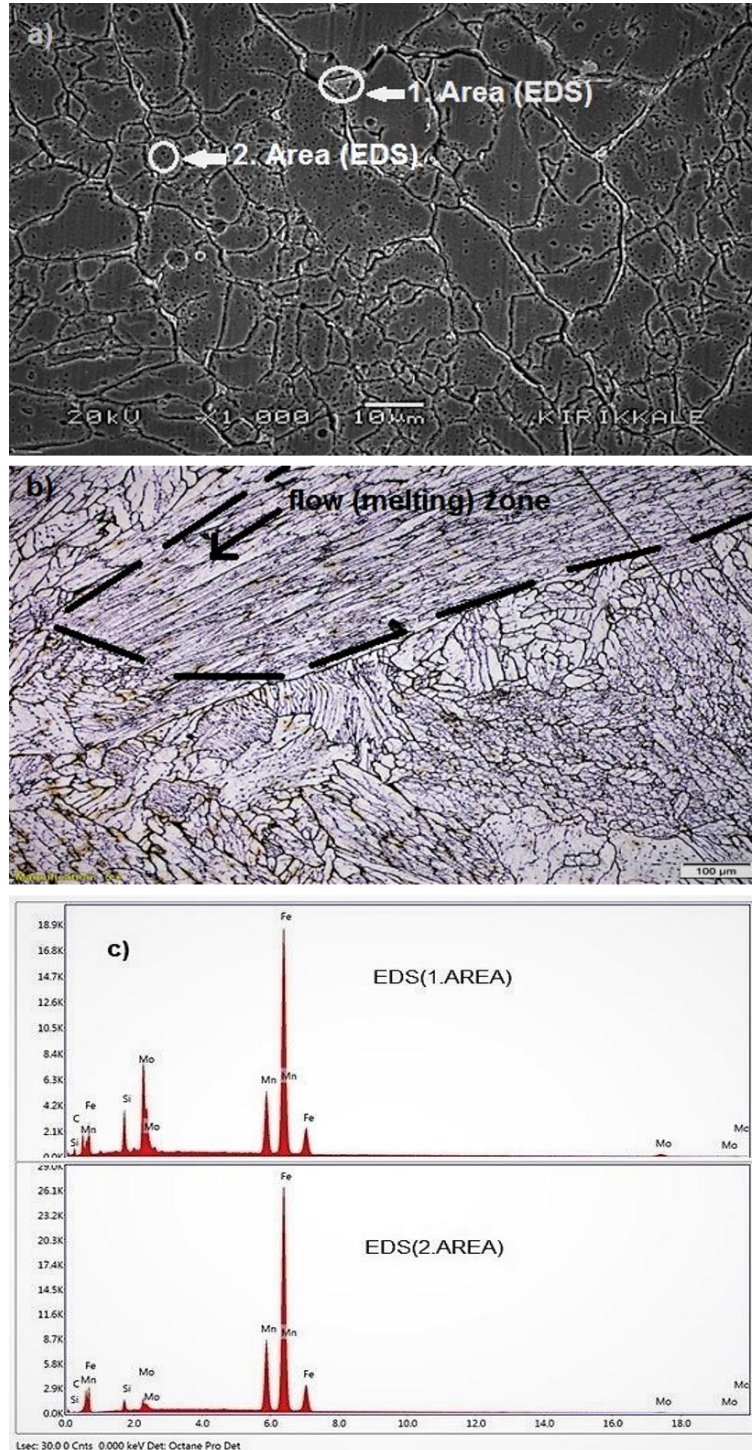
Figure 2. Ferrite grain structure in Fe–18.45 wt.% Mn–4.69 wt.% Mo–1.99 wt.% Si alloy and microstructure images showing selected areas for EDS (a) SEM, (b) MM, (c) EDS peaks taken from selected regions
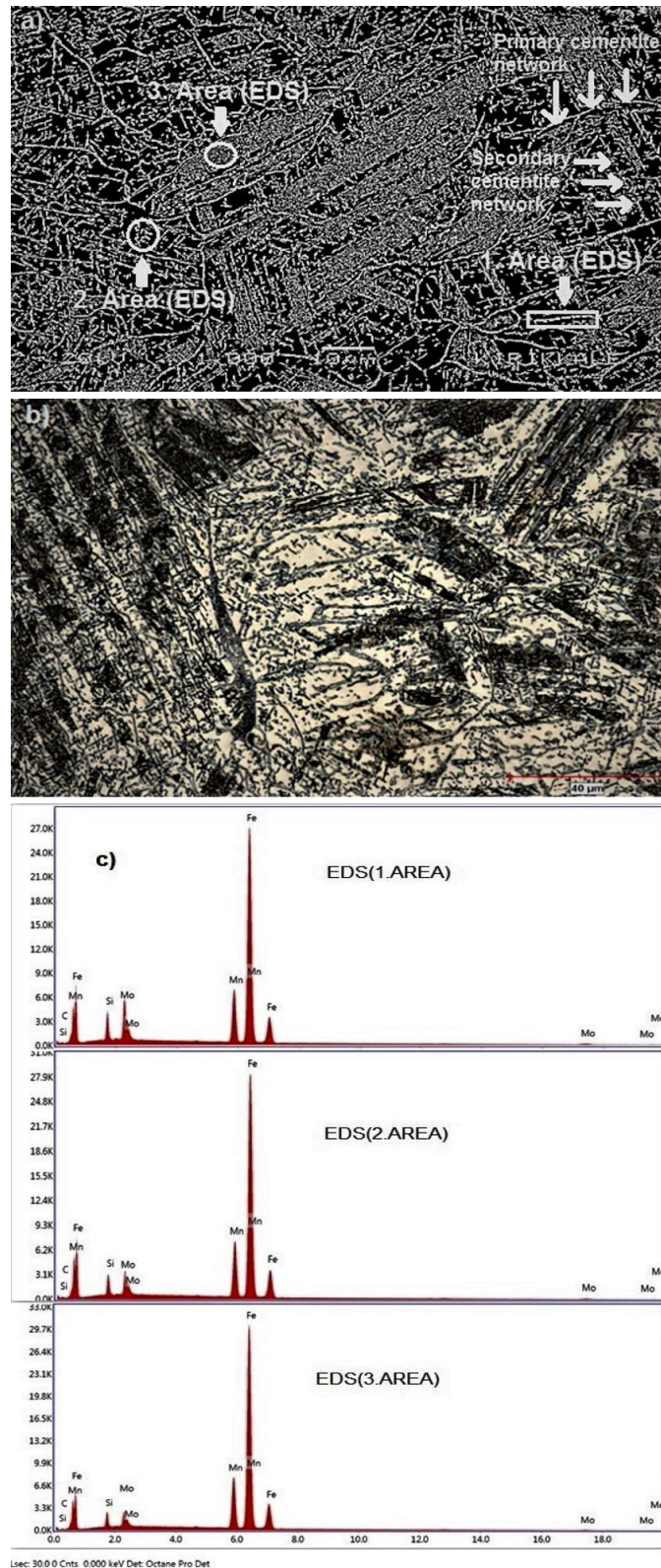
Figure 3. Pearlite phase and cementite network belonging to A_2 sample and microstructure images showing selected areas for EDS (a) SEM, (b) MM, (c) EDS peaks taken from selected regions

formation can be observed in fast–cooled alloys in excess Mn. In previous studies, it has been observed that although the amount of bainite formation in the samples subjected to rapid cooling is low, all of the slow cooled samples are transformed into bainite structure [39]. The EDS analysis results of the 1st and 2nd regions marked as circular in Figure 1a show

that the amount of C (wt.%) increases (in Table 3). Accordingly, it is believed that carbon in the 1st zone is combined with carbide–forming elements such as Fe and Mo to form bainitic–ferrite lamellae which are formed in the boundaries of the grain and growed intensively. In the EDS analysis of the 2nd region, there was a very large decrease in the amount of Mo

(wt.%) and it could be said that this area, which is known as retained austenite, is caused by the excess Mn element.

The SEM and MM images of the B_1 sample were given in Figure 2(a, b). In the micro–images of Figure 2, the ferrite grains formed in the austenite grain boundaries are noteworthy. Ferrite structures begin to nucleate from the austenite grain boundaries and grow over time to produce large and small ferrite precipitations. Ferrite is usually a solid solution of iron containing carbon or one or more alloying elements (Si, Cr, Mn, Ni, etc.) [5, 10–14]. In Figure 2a, based on the results of the EDS analysis from the 1st region, it was understood that there was a significant decrease in Fe and Mn elements according to the data obtained from the precipitate in the grain boundary. It is thought that C atoms that are excluded from the ferrite structure are clustered in this region of the precipitate and formed in the Fe_3C (or Mo_2C) precipitate. According to the results EDS analysis of the 2nd region, the reason for the decrease in Mo and Si can be explained as the fact that these element atoms cannot diffuse into the structure, and they are present as carbide forming elements in the precipitates in the grain boundaries.

As reported in the literature, both ferrite and cementite begin to nucleate from the austenite grain boundaries [4, 10, 11, 24]. The excess carbon in iron forms the cementite iron carbide compound. Depending on the amount of C (wt.%) in the alloy, some of its elements are partially soluble in ferrite and some partly form carbide. Nb, Ti, W, V, Mo are strong carbide forming elements (Mo_2C). Mn is also capable of forming carbide with carbon (Mn_3C) [40–42]. In general, a structure with a carbon content less than 0.02% can be defined as a ferrite. In a similar study, Al–Abbasi [43], observed almost 3% pearlite phase with single phase ferrite throughout the structure. Since the carbon content is very low, pearlite does not have any importance in the overall behavior of the phase. Also they observed that cementite precipitates in the ferrite grain boundaries [43].

Although the homogenization temperature and cooling method did not change, the bainite formation in the A_1 sample was not observed in the B_1 sample. The main reason for this situation is the increase in the rate of Mn (wt.%). As it is known, Mn austenite is a stabilizing element and diffusion to ferrite is also difficult. Therefore, due to the effects of C (wt.%) and other alloying elements, bainite structure was not formed in the B_1 sample [44–46].

In Figure 2b, ferrite grains were observed at the regions adjacent to the melting zone (Sample B_1). Ferrite diffusion increased during the heat treatment period and it seems to cover the structure completely [47]. In a similar study, Yuan et al. showed that the ferrite diffusion takes place along the austenite grain boundaries along the flow zone [48].

SEM and MM image of A_2 sample is given in Figure 3(a, b). In these micro photographs, retained austenite and pearlite (ferrite and cementite) were observed together. While pearlite formation is present in the cementite network, the black regions are ferrite or austenite residues (dark regions separated by iron carbide white strips are pearlite). In the study of high–carbon steels, cementite strips, which determine pearlite grains, are similar to the microstructure shown in Figure 3 [49]. According to the EDS analysis taken from the 3 regions marked in Figure 3a, it was observed that the percentage distribution of the element in the alloy changed significantly according to the overall alloy composition (in Table 3). The increase in the distribution of Mn, Si and C is observed in EDS analysis of this sample where cementite formation is observed intensively.

With the increase of the heat treatment temperature in the A_2 sample, the structure became saturated with carbon and the excess of the carbon present in the alloy formed the iron carbide compound. The carbon ratio in this alloy is approximately 0.015 (wt.%). Although the carbon content is very low, the alloying elements affect the percentage of carbon required to initiate phase conversion. Thus, the percentage of carbon required to initiate the pearlite conversion is considerably reduced. The amount of carbon contained in the alloy is chemically anchored in the form of iron carbide and is in the form of a cementite [41, 42]. Carbon dissolves in iron showing allotropic structure (the same element is present in different crystal structures at different temperatures) and forms different intermediate solid solutions [10, 50]. Depending on whether all the carbon except the solid solution forms an intermediate compound (Fe_3C) with iron or is completely in the form of free graphite (C), either the iron–cementite or iron–graphite binary microstructure is involved [49]. After heat treatment, a carbon–iron phase precipitate is formed around the austenite grains, which are saturated with carbon by fast cooling (Figure 3b) and the remaining austenite becomes pearlite [51–53]. As a result, pearlite zones are surrounded by a cementite structure. This is a dense and reticulated cementite primary cementite network. Cementite particles or cementite plates that are dispersed in the grain are known as secondary cementite [49].

The SEM and MM images of B_2 were given in Figure 4(a, b). As in the sample A_2 treated with the same heat treatment temperature, the cementite web–wrapped pearlite structure was also seen in this sample. The results of EDS analysis of 1st and 2nd regions are given in Table 3. The density of the cementite in the structure can be interpreted as the fact that the Mn element, with its rapid cooling effect,
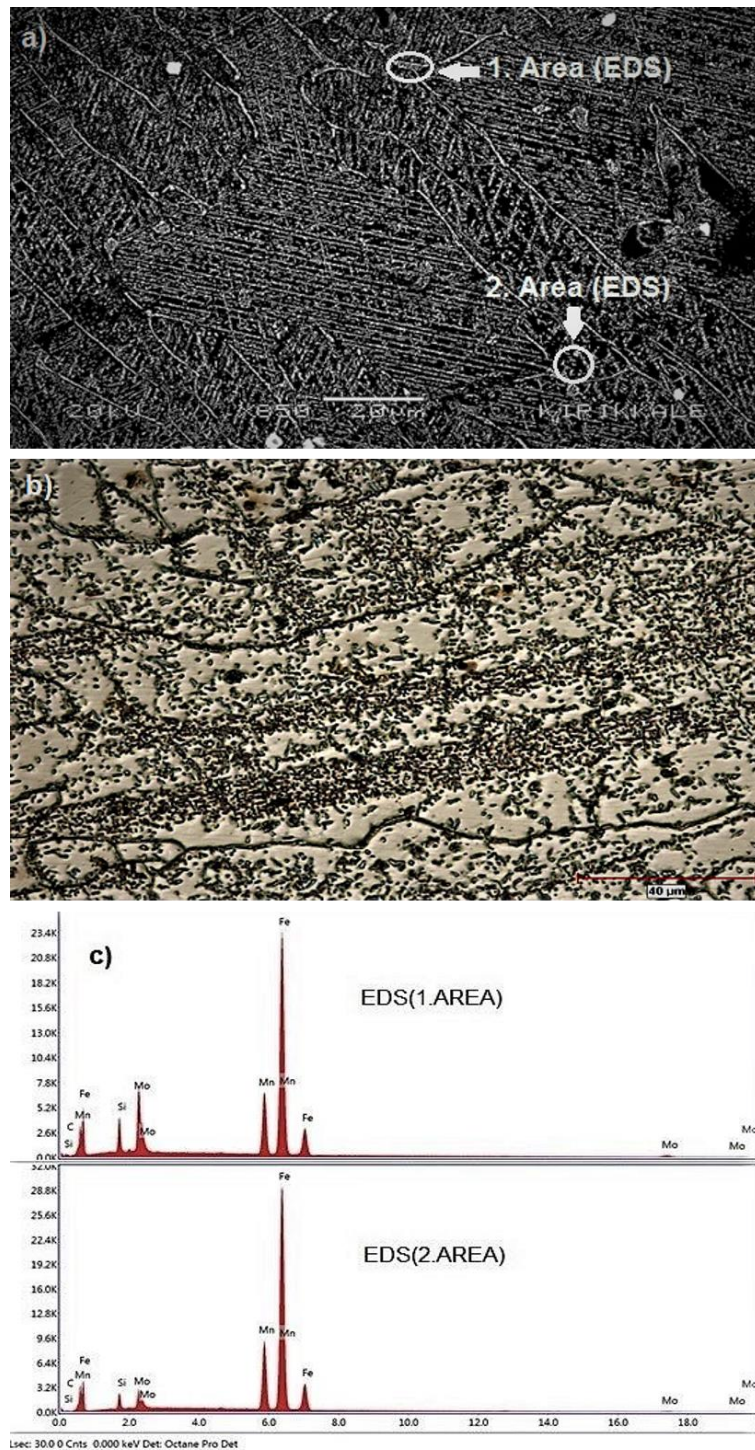
Figure 4. Microstructure image of samples belonging to Fe–18.45 wt.% Mn–4.69 wt.% Mo–1.99 wt.% Si of homogenized at 900 °C for 2 h and quenched in water bath at room temperature (a) SEM, (b) MM, (c) EDS peaks taken from selected regions

is able to reveal its cementite–forming property thanks to its more intense Mn ratio. In a similar study by Larn R.H., bundle–like bainitic structures were also found along with the dense cementite network [54].

3.2. TEM observations

When the TEM image of the A_1 sample is examined, it is seen that the dark block regions are bainitic ferrite (BF) and the regions with dislocation webs are

residual austenite (Figure 5). The analysis of the electron diffraction pattern taken from the marked region confirmed that f.c.c.→b.c.c. transformation occurred (Figure 5) [37]. The formation of large amounts of dislocation (D) network within the Austenite phase means that dislocations play a role in the formation of BF. Bainite grows without any spread and is separated into the austenite immediately after the carbon conversion. In this case, dislocations in the austenite phase can be transformed into a bainite structure [30, 55–57].

Crystallography of phase transformation in low–carbon alloys and the orientation relationship between austenite with bainite conform to the K–S relationship [58–63]. Although the real orientation relationships between the two phases are irrational, can produce up to 24 different ferrite variants in a single austenite in the K–S relationship [62]. Variants with planes close to the same parallel as Austenite belong to the same type of crystallographic package. By measuring the distances between the reflecting planes in the electron diffraction pattern given in Figure 5 (using equation 1) was calculated lattice constants for f.c.c. and b.c.c. structures (f.c.c. for structure $a_\gamma \cong 3.5853$ Å and b.c.c. for the structure $a_\alpha \cong 2.8567$ Å). Crystallographic analysis carried out the on selected area diffraction pattern revealed a K–S type orientation relationship between bainitic structure and austenite phase. As can be seen in Figure 5 the orientation between austenite and bainite phases are in the form of $(\bar{1}11)_\gamma//(011)_\alpha$ parallelism with $[101]_\gamma//[\bar{1}1\bar{1}]_\alpha$ directions.

electron diffraction pattern analysis, the lattice parameter; for the b.c.c. structure was calculated as 2.9885 Å.

Figure 6. Bright field TEM image and electron diffraction pattern belonging to ferrite phase for sample B_1
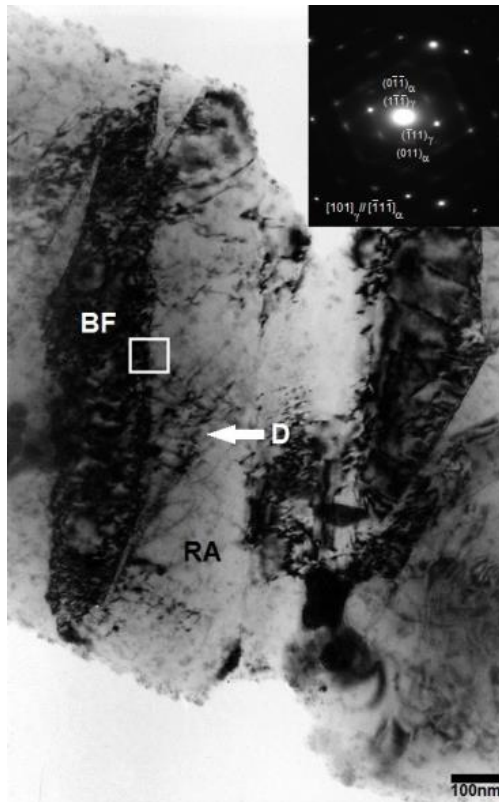
Figure 5. Bright field TEM image and electron diffraction pattern obtained from the selected area (BF : Bainitic-Ferrite and RA : Retained Austenite) for sample A_1 in Fe–15.14 wt.% Mn–5.10 wt.% Mo–2.18 wt.% Si alloy

The TEM image of the ferrite and austenite structures and the electron diffraction pattern taken from the ferrite structure were given in Figure 6 (Sample B_1). In the SEM image given in Figure 2, it was found that the ferrite product phase was formed. According to the electron diffraction pattern analysis result, it was understood that ferrite had crystallized in b.c.c structure. In Figure 6, by measuring the distances d between the reflecting planes according to the

Figure 7. Bright field TEM image showing ε martensite plates and precipitates and electron diffraction pattern belonging to precipitate (sample A_2)

427
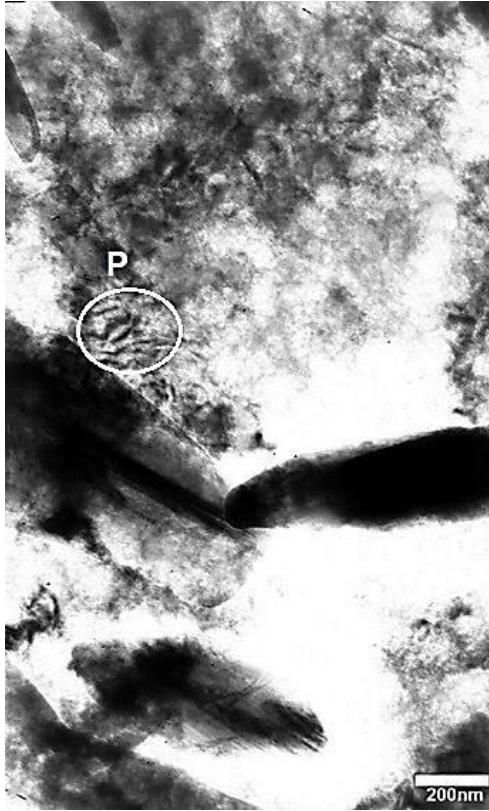
Figure 8. Bright field TEM image belonging to pearlite phase for sample B_2 in Fe–18.45 wt.% Mn–4.69 wt.% Mo–1.99 wt.% Si (P : Pearlite)

The TEM image of the A_2 sample and the index diagram with the electron diffraction pattern are given in Figure 7. Cementite precipitation and epsilon phase were observed in the regions marked with this micro–photo. Lattice constants using electron diffraction pattern analysis taken over the precipitate phase; For cementite lattice parameter were obtained as $a_\theta \cong 4.6126$ Å, $b_\theta \cong 4.9458$ Å and $c_\theta \cong 6.4941$ Å. The TEM image of the B_2 sample is given in Figure 8. The cementite precipitate was found as in the A_2 sample at the same heat treatment temperature. Pearlite (P) formation was observed in the marked region.

3.3. XRD analysis

The XRD patterns of the samples are demonstrated in Figure 9 (a–d). The peak of diffraction giving plane $(110)_\alpha$ of the bainite structure for the A_1 sample was clearly observed. The peaks belonging to diffraction giving planes $(110)_\alpha$ and $(200)_\alpha$ of the ferrite phase for the B_1 sample and the peaks belonging to diffraction giving planes of austenite phase were

determined. For the A_2 sample, the peaks of the diffraction giving planes of cementite and ferrite phases revealed by TEM analyzes were shown in Figure 9c. The peaks belonging to diffraction giving planes $(112)_\theta$, $(021)_\theta$, $(103)_\theta$ and $(122)_\theta$ of cementite phase were observed for both A and B samples. At the same time, the peaks belonging to diffraction giving planes $(100)_\varepsilon$ and $(110)_\varepsilon$ of the ε phase (h.c.p.) observed in the TEM images were also given for the A_2 sample. For the B_2 sample, the peaks of diffraction giving planes $(110)_\alpha$, $(200)_\alpha$ of the b.c.c. structure belonging to the ferrite phase and the peak of diffraction giving plane $(100)_\varepsilon$ of the h.c.p. structure belonging to the martensite phase were given. In addition, the knitting parameters of these structures were calculated and given in Table 4 by using the analysis of these obtained planes.
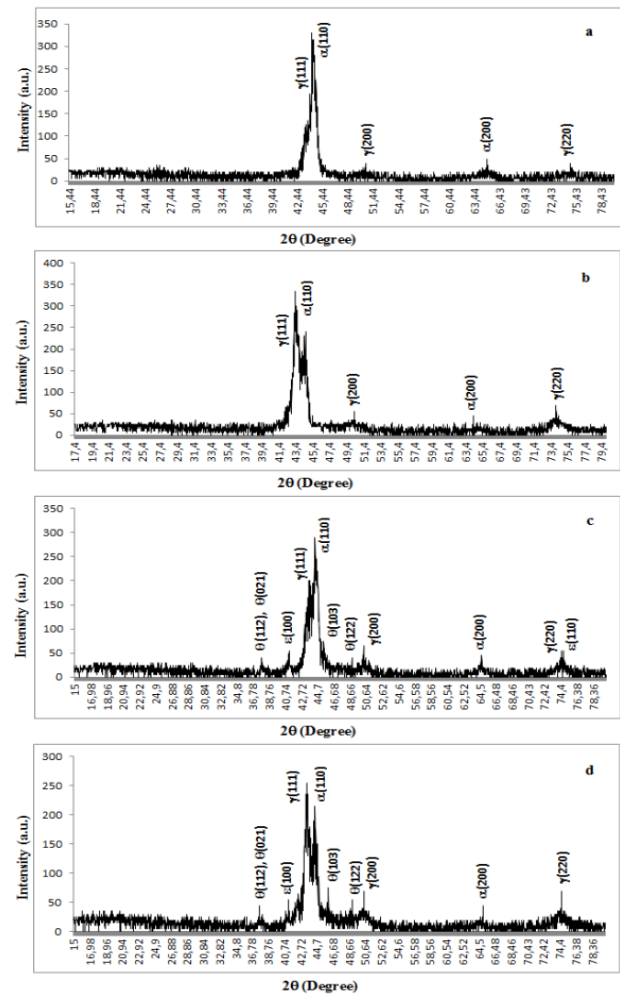
Figure 9. XRD measurements of thermally induced phase transformations (a) A_1, (b) B_1, (c) A_2, (d) B_2

Table 4. The lattice parameter of austenite and bainite, ferrite, cementite in A and B alloys

Alloys	Lattice parameters (A°)				
	γ phase	α phase	θ phase		
	(a_γ)	(a_α)	(a_θ)	(b_θ)	(c_θ)
A_1	3.6066	2.8818	––	––	––
B_1	3.6222	2.8707	––	––	––
A_2	3.6088	2.8745	4.4329	4.9507	6.6592
B_2	3.6298	2.8743	4.4856	5.0898	6.7419

4. Conclusion

In this study, the effects of homogenization temperature on microstructure and crystallographic properties of Fe–X (wt.%) Mn–Mo–Si (X = 15.14% and 18.45%) alloys were investigated. Results obtained are given below.

1. The microstructures of the heat treated samples were revealed in SEM investigations. Bainitic–ferrite structure in A_1 sample, ferrite structure in B_1 sample, pearlite structure in A_2 and B_2 samples were observed.
2. In the TEM analyzes of the A_1 sample, it was understood that the bainite phase had crystallized in the structure b.c.c. The orientation relationship for $\gamma \rightarrow \alpha$ was obtained as

$$(\bar{1}11)_\gamma//(011)_\alpha \, , \, [101]_\gamma//[\bar{1}1\bar{1}]_\alpha$$

Also, as a result of analysis of the electron diffraction pattern, it was reported that B_1 sample was crystallized as ferrite (b.c.c.) while A_2 and B_2 samples were crystallized in a cementite (orthorhombic) structure.

3. The lattice parameters belonging to microstructures of bainite, ferrite, cementite and austenite phases observed in TEM and SEM investigations were calculated by using XRD analysis results (Table 4).

Acknowledgment

Declaration of Ethical Code

In this study, we undertake that all the rules required to be followed within the scope of the "Higher Education Institutions Scientific Research and Publication Ethics Directive" are complied with, and that none of the actions stated under the heading "Actions Against Scientific Research and Publication Ethics" are not carried out.

References

[1] Chowdhury, P., Canadinc, D., Sehitoglu, H. 2017. On deformation behavior of Fe-Mn based structural alloys. Materials Science and Engineering R Reports, 122, 1–28.

[2] Kirindi, T., Guler, E., Dikici, M. 2007. Effects of homogenization time on the both martensitic transformations and mechanical properties of Fe–Mn–Si–Cr–Ni shape memory alloy. Journal of Alloys and Compounds, 433, 202–206.

[3] Nishiyama, Z. 1978. Martensitic Transformations. 1nd edition. Academic Press. New York, 6s.

[4] Christian, J. W. 1975. The Theory of Transformation in Metals and Alloys. 2nd, the first part of that edition was revised and re-published. Pergamon Press. London, 813s.

[5] Wegst, C. W. 1986. Stahlschlüssel. 14nd edition. Verlag Stahlschlüssel Wegst Gmbh. Germany, 112s.

[6] Moffatt, W. G., Pearsall, G. W., Wulff, J. 1964. The structure and properties of materials, structure, part1. 1nd edition. John Wiley and Sons. New York, 134s.

[7] Brophy, J.H., Rose, R.M., Wulff J. 1964. The structure and properties of materials, thermodynamics, part2. 1nd edition. John Wiley and Sons. New York, 113s.

[8] Smith, W. F. 1986. Principles of Materials Science and Engineering. 1nd edition. McGraw-Hill. New York, 325s.

[9] Askeland, D. R., Webster, P. 1990. The Science and Engineering of Materials. 2nd edition. Chapman and Hall. London, 430s.

[10] Dieter, G., E. 1997. Effects of Composition, Processing, and Structure on Properties of Irons and Steels. Materials Selection and Design, Vol 20, ASM Handbook, ASM International, USA, 125s.

[11] Bain, E. C. 1932. Factors affecting the inherent hardenability of steel. Transactions of the American Society for Steel Treating, 20, 385-428.

[12] Bhadeshia, H. K. D. H., Christian, J. W. 1990. Bainite in stells. Metallurgical and Materials Transactions A, 21, 767–797.

[13] Irvine, K. J., Pickering, F. B. 1957. Low-carbon bainitic stells. Journal of the Iron and Steel Institute, 187, 292-309.

[14] Caballero, F. G., Bhadeshia, H. K. D. H., Mawella, K. J. A., Jones, D. G., Brown, P. 2002. Very Strong Low Temperature Bainite. Materials Science and Technology, 18, 279–284.

[15] Chang, L. C. 2004. Microstructures and reaction kinetics of bainite transformation in Si-rich stells. Materials Science and Engineering A, 368(1-2), 175-182.

[16] Srinivasan, G. R., Wayman, C. M. 1968. Transmission electron microscope study of the bainite transformation in iron-chromium-carbon alloys. Acta Metallurgica, 16(5), 609-620.

[17] Bhadeshia, H. K. D. H., Edmonds, D. V. 1980. The mechanism of bainite formation in steels. Acta Metallurgica, 28(9), 1265-1273.

[18] Greninger, A. B. Troianao, A. R. 1940. Crytallography of austenite decomposition. Trans. AIMME, 140, 307-336.

[19] Tsuzaki, K., Maki, T. 1995. Some Aspects of Bainite Transformation in Fe-Based Alloys. Journal de Physique, 5, 61-70.

[20] Klier, E. P. Lyman, T. 1944. The bainite reaction in hypoeutectoid steels. Trans. AIMME, 158, 394-422.

[21] Bhadeshia, H. K. D. H. 2001. Bainite in Steells. 2nd edition. The University Press. Cambridge, London, 63s.

[22] Zhang, M. X., Kelly, P. M. 2002. Accurate orientation relationship between ferrite and austenite in low carbon martensite and granular bainite. Scripta Materialia, 47, 749-755.

[23] Bhadeshia, H. K. D. H., Edmonds, D. V. 1979. The Bainite Transformation in a silicon steel. Metallurgical and Materials Transactions A, 10, 895–907.

[24] Lee, C. H., Bhadeshia, H. K. D. H., Lee, H. C. 2003. Effect of plastic deformation on the formation of acicular ferrite. Materials Science and Engineering A, 360, 249-257.

[25] Arici, G., Acarer, M., Uyaner, M. 2021. Effect of Co addition on microstructure and mechanical properties of new generation 3Cr-3W and 5Cr-3W steels. Engineering Science and Technology, an International Journal, 24(4), 974-989.

[26] Arici, G., Acarer, M., Uyaner, M. 2019. 3 ve 5 kromlu çeliklerde tantalyum ve krom ilavesinin mikroyapıya ve çentik darbe direncine etkisi. Selçuk-Teknik Dergisi, 18(3), 241-252.

[27] Tan, X., Xu, Y., Yang, X., Liu, Z., Wu, D. 2014. Effect of partitioning procedure on microstructure and mechanical properties of a hot-rolled directly quenched and partitioned steel. Materials Science and Engineering A, 594, 149–160.

[28] Tan, X., Xu, Y., Yang, X., Wu, D. 2014. Microstructure properties relationship in a onestep quenched and partitioned steel. Materials Science and Engineering A, 589, 101–111.

[29] Mijovilovich, A., Goncalves Vieira, A., Paniago, R., Pfannes, H. D., Mendonc Gonzalez, B. 2000. Mössbauer study of the retained austenitic phase in multiphase steels. Materials Science and Engineering A, 283, 65-69.

[30] Xing, X. L., Zhou, Y. F., Yang, Y. L., Gao, S. Y., Ren, X. J., Yang, Q. X. 2015. Surface modification of low-carbon nano-crystallite bainite via laser remelting and following isothermal transformation. Applied Surface Science, 353, 184–188.

[31] Batz, W., Mead, H. W., Birchenall, C. E. 1952. Diffusion of Silicon in Iron. Journal of Metals, 4(10), 1070.

[32] Weber, E. R. 1983. Transition metals in silicon. Applied Physics A, 30(1), 1–22.

[33] Maalekian, M. 2007. The effects of alloying elements on steels. https://online.tugraz.at/tug_online/voe_main2.getvolltext?pCurrPk=32837 (Erişim Tarihi: 18.02.2021).

[34] Aksoy, M., Kuzucu, V., Korkut, M. H. 1997. The influence of strong carbide-forming elements and homogenization on the wear resistance of ferritic stainless steel. Wear, 211, 265-270.

[35] Kuzucu, V., Aksoy, M., Korkut, M. H. 1998. The effect of strong carbide-forming elements such as Mo, Ti, V and Nb on the microstructure of ferritic stainless steel. Journal of Materials Processing Technology, 82, 165–171.

[36] Barford, J., Owen, W. S. 1962. The effect of austenite grain size and temperature on the rate of bainite transformation. Metal Science and Heat Treatment, 4, 359–360.

[37] Umemoto, M., Horiuchi, K., Tamura, I. 1982. Transformation Kinetics of Bainite during Isothermal Holding and Continuous Cooling. Tetsu-to-Hagane, 68, 461–470.

[38] Graham, L. W., Axon, H. J. 1959. The Effect of Austenitising Treatments on Formation of Lower Bainite in a Plain Carbon Steel. The Journal of the Iron and Steel Institute, 191, 361–365.

[39] Gao, G., Zhang, H., Tan, Z., Liu, W., Bai, B. 2013. A carbide-free bainite/martensite/austenite triplex steel with enhanced mechanical properties treated by a novel quenching–partitioning–tempering process. Materials Science and Engineering A, 559, 165–169.

[40] Kral, M. V. Spanos, G. 1999. Three-dimensional analysis of proeutectoid cementite precipitates. Acta Materialia, 47(2), 711-724.

[41] Kral, M. V., Spanos, G. 2003. Crystallography of grain boundary cementite dendrites. Acta Materialia, 51, 301–311.

[42] Mangan, M. A., Kral, M. V. Spanos, G. 1999. Correlation between the crystallography and morphology of proeutectoid widmanstatten cementite precipitates. Acta Materialia, 47(17), 4263-4274.

[43] Al-Abbasi, F. M. 2010. Micromechanical modeling of ferrite-pearlite steels. Materials Science and Engineering A, 527, 6904–6916.

[44] Wang, J., Van der Wolk, P., Van der Zwaag, S. 2000. On the influence of alloying elements on the bainite reaction in low alloy steels during continuous cooling. Journal of Materials Science, 35, 4393–4404.

[45] Chen, H., Zhu, K., Zhao, L., Van der Zwaag, S. 2013. Analysis of transformation stasis during the isothermal bainitic ferrite formation in Fe–C–Mn and Fe–C–Mn–Si alloys. Acta Materialia, 61, 5458–5468.

[46] Chen, H., Borgenstam, A., Odqvist, J., Zuazo, Goune, M., Agren, J., Zwaag, S. 2013. Application of interrupted cooling experiments to study the mechanism of bainitic ferrite formation in steels. Acta Materialia, 61, 4512–4523.

[47] Palmer, T. A., Elmer, J. W., Babu, S. S. 2004. Observations of ferrite/austenite transformations in the heat affected zone of 2205 duplex stainless steel spot welds using time resolved X-ray diffraction. Materials Science and Engineering A, 374, 307–321.

[48] Yuan, F., Bian, X., Jiang, P., Yang, M., Wu, X. 2015. Dynamic shear response and evolution mechanisms of adiabatic shear band in an ultrafine-grained austenite-ferrite duplex steel. Mechanics of Materials, 89, 47–58.

[49] Colvın, F.H. 2007. The working of steel annealing, heat treating and hardening of carbon and alloy steel. 2nd Edition. Mcgraw-Hıll Book Company. New York, 22s.

[50] Goune, M., Danoix, F., Agren, J., Brechet, Y., Hutchinson, C.R., Militzer, M., Purdy, G., Van der Zwaag, S., Zurob, H. 2015. Overview of the current issues in austenite to ferrite transformation and the role of migrating interfaces therein for low alloyed steels. Materials Science and Engineering R Reports, 92, 1–38.

[51] Miyamoto, G., Karube, Y., Tadashi Furuhara, T. 2016. Formation of grain boundary ferrite in eutectoid and hypereutectoid pearlitic steels. Acta Materialia, 103, 370-381.

[52] Shimizu, K., Kawabe, N. 2001. Size dependence of delamination of high-carbon steel wire. ISIJ International, 41, 183-191.

[53] Oki, Y., Ibaraki, N., Ochiai, K., Minamida, T., Makii, K. 2000. Microstructure influence on ultra high tensile steel cord filament delamination. R&D Kobe Steel Engineering Reports, 50, 37-41.

[54] Larn, R. H., Yang, J. R. 2000. The effect of compressive deformation of austenite on the bainitic ferrite transformation in Fe-Mn-Si-C steels. Materials Science and Engineering A, 278, 278–291.

[55] Caballero, F. G., Miller, M. K., Garcia-Mateo, C., Cornide, J. 2013. New experimental evidence of the diffusionless transformation nature of bainite. Journal of Alloys and Compounds, 577, 626–630.

[56] Hulme-Smith, C. N., Lonardelli, I., Dippel, A. C., Bhadeshia, H.K.D.H. 2013. Experimental evidence for non-cubic bainitic ferrite. Scripta Materialia, 69, 409–412.

[57] Caballero, F. G., Miller, M. K., Garcia-Mateo, C., Capdevila, C., Babu, S. S. 2008. Redistribution of alloying elements during tempering of a nanocrystalline steel. Acta Materialia, 56, 188–199.

[58] Morito, S., Tanaka, H., Konishi, R., Furuhara, T., Maki T. 2003. The morphology and crystallography of lath martensite in Fe–C alloys. Acta Materialia, 51, 1789–1799.

[59] Kitahara, H., Ueji, R., Tsuji, N., Minamino, Y. 2006. Crystallographic features of lath martensite in low-carbon steel. Acta Materialia, 54, 1279–1288.

[60] Furuhara, T., Kawata, H., Morito, S., Miyamoto, G., Maki T. 2008. Variant selection in grain boundary nucleation of upper bainite. Metallurgical and Materials Transactions A, 39, 1003–1013.

[61] Lambert-Perlade, A., Gourgues, A. F., Pineau, A. 2004. Austenite to bainite transformation in the heat-affected zone of a high strength low alloy steel. Acta Materialia, 52, 2337–2348.

[62] Pereloma, E. V., Al-Harbi, F., Gazder, A. A. 2014. The crystallography of carbide-free bainites in thermo-mechanically processed low Si transformation-induced plasticity steels. Journal of Alloys and Compounds, 615, 96-110.

[63] Takayama, N., Miyamoto, G., Furuhara, T. 2012. Effects of transformation temperature on variant pairing of bainitic ferrite in low carbon steel. Acta Materialia, 60, 2387–2396.